High efficiency black silicon Interdigitated Back Contacted solar cells on p- and n-type c-Si substrates

Pablo Ortega[1], Eric Calle[1], Guillaume von Gastrow[2], Päivikki Repo[2], David Carrió[1], Hele Savin[2], Ramón Alcubilla[1]

[1] Universitat Politècnica de Catalunya, Dept. Enginyeria Electrònica, C/ Jordi Girona 1-3, Modul C4, E - 08034 Barcelona, Spain

[2] Aalto University, Department of Micro- and Nanosciences, Tietotie 3, 02150 Espoo, Finland

Abstract

This work demonstrates the high potential of Al_2O_3 passivated black silicon in high efficiency Interdigitated Back Contacted (IBC) solar cells by reducing surface reflectance without jeopardizing surface passivation. Very low reflectance values, below 0.7% in the 300-1000 nm wavelength range, together with striking surface recombination velocities values of 17 and 5 cm/s on p- and n-type crystalline silicon substrates respectively, are reached. The simultaneous fulfillment of both requirements, low reflectance and low surface recombination, paves the way for the fabrication of high efficiency interdigitated back contacted Si solar cells using black silicon at their front surface. Outstanding photovoltaic efficiencies over 22% have been achieved both in p- and n-type, 9 cm^2 cells. 3D simulations suggest that efficiencies up to of 24% can be obtained in the future with minor modifications in the baseline fabrication process.

Keywords: black silicon, crystalline silicon, IBC solar cell, high efficiency, ALD Al_2O_3, passivation

1. Introduction

Interdigitated Back Contacted (IBC) crystalline Silicon solar cells allow excellent photovoltaic conversion efficiencies [1-3], in particular a new world record efficiency of 25.6% in large area n-type device has been recently obtained [4]. In IBC cells, both base and emitter regions with their corresponding electrodes are alternated in a strip-like fashion at the backside of the cell, whereas light impinges on the front device surface. Some advantages of this structure are evident, the absence of metal shadow losses and the facility to assemble solar cells in modules with coplanar connection. However, if one wants to exploit the full benefit of this structure, high minority-carrier bulk lifetime, outstanding front and rear surface passivation [5, 6], and low front reflectance are mandatory.

Very low reflectance values in the whole solar spectrum wavelength range can be achieved by nanostructuring front cell surface through so-called black silicon etching (b-Si) [7]. Another advantage of b-Si is to maintain excellent low reflectance values for a broad range of light incidence angles, which offers a potential for daily and yearly photovoltaic energy production increase [8]. However, as a result of black silicon formation the surface area greatly increases and consequently the recombination at the surface becomes a critical issue. It is well known that Al_2O_3 films achieve outstanding passivation on planar and textured n- and p-type c-Si due to both chemical and field effect passivation [9, 10]. Regarding surface passivation of b-Si, very promising results using atomic layer deposited ALD Al_2O_3 have been reported recently on both types of substrate polarities [11-13]. Additionally, ALD Al_2O_3 material is also a high optical bandgap material (~6.5 eV) [10] with scarcely light absorption in the whole solar spectrum wavelength range [14], paving the way for applying nanostructures to the front surface of the IBC cell architecture (b-Si IBC cell from now on).

In a recent work, we have demonstrated high efficiency b-Si IBC solar cells (>22%) on p-type FZ c-Si substrates (9 cm^2 cell area) using b-Si passivated with ALD Al_2O_3 at the front surface [8]. However the negative charge within the Al_2O_3 layer accumulates or inverts the silicon surface on p- and n-type material respectively; thus it remains unclear if the overall surface passivation of b-Si on n-type will reach the same excellent values

as on p-type b-Si surface in finished IBC's solar cells. In fact, no efficiencies over 20% have been yet reported for n-type b-Si IBC's [15-17].

It is especially relevant to explore n-type b-Si IBC cells because it is the material of choice of IBC's high efficiency solar cell manufacturers for a number of reasons: on one hand because, unlike p-type substrates, this material do not exhibit light induced degradation (LID) by the formation of boron-oxygen complexes [18]. On the other hand, n-type substrates are less sensitive to the degradation of charge carrier lifetime due to recombination-active metal impurities (e.g. iron contamination) exhibiting higher stable lifetimes than p-type c-Si [3].

In this work we extend our previous results on p-type b-Si IBC cells [8] to n-type substrates. Surface passivation of b-Si nanostructures and photovoltaic b-Si IBC cell parameters are directly compared and analyzed for both types of substrates. 3D simulations will help y to detect the main efficiency loss mechanisms giving clues to improve both p- and n-type b-Si IBC cells.

2. Black silicon etching. Reflectance and surface passivation

2.1 Experimental

In order to assess the reflectance of b-Si and its surface passivation we use conventional randomly textured surfaces as a reference. High quality defect free crystalline silicon FZ <100> oriented 2.7±0.2 Ωcm 4 inches wafers (285±15 μm thick) were used in the experiments.

Black silicon was etched through a cryogenic inductively coupled plasma reactive-ion etching process (ICP-RIE) at -120 ºC using SF_6 and O_2 as etching gases. Reference cells were textured by anisotropic etching in tetramethylammonium hydroxide (TMAH), isopropanol (IPA) and DI water (320 ml:350 ml:3300 ml) at 80ºC resulting in random pyramids. After the etch, the wafers were RCA cleaned and HF-dipped before the atomic layer deposition of 20 or 90 nm thick Al_2O_3 layers at 200ºC for the b-Si and reference samples respectively. In the ALD process, TMA was used as the aluminum

source and water as the oxidant. Surface passivation has been monitored using symmetrically treated samples. Reflectance has been characterized on samples etched only on the front side with a back reflector scheme of thermally grown dry SiO_2 (110 nm) and aluminum Al (2 μm) deposited by e-beam. A final forming gas annealing at 400ºC for 10 min was performed in all cases.

As can be seen in Fig. 1, the black silicon etching results in a morphology consisting of pillars densely and randomly distributed in the silicon surface with heights and base widths of less than 1 μm and 200 nm respectively. Only 1 μm of silicon was etched before the actual b-Si formation. Therefore this technique is very well suited to ultrathin crystalline Silicon solar cells (< 10 μm) [19] where conventional surface texturing is not possible due to relative high silicon consumption in the etching (~20 μm), as well as an alternative to acidic etching on mc-Si substrates [11].

<Fig.1>

2.2 Reflectance measurements

Reflectance measurements were made using a UV-VIS-NIR spectrometer (Shimadzu 3600) with integrating sphere. Fig. 2 shows the reflectance R of two samples, one of them b-Si etched and the other textured with random pyramids. The spectral photon flux density $\phi_{AM1.5}$ corresponding to the AM1.5G solar spectrum is also depicted in the graph for comparison. Black silicon nanostructures exhibit a very low reflectance, below 0.7% in the 300-1000 nm wavelength range, clearly lower than the reference with random pyramids in the UV and blue part of the spectrum.

<Fig.2>

Using these reflectance results, one could estimate in both cases the maximum short-circuit current density $J_{sc,max}$ of a hypothetical solar cell assuming zero transmittance, i.e ideal back reflector, and an ideal internal quantum efficiency as follows

$$J_{sc,max} \cong q \int_{300\ nm}^{1130\ nm} \phi_{AM1.5}(\lambda) \times (1 - R(\lambda)) d\lambda \quad (1)$$

where q is the elementary charge and the integral is evaluated in the useful absorption wavelength range in c-Si under AM1.5G solar spectrum, i.e. 300-1130 nm. For b-Si surface $J_{sc,max}$ reaches 43.5 mA/cm^2, 0.5 mA/cm^2 more than its texturized counterpart (43.0 mA/cm^2), or 1 mA/cm^2 less compared with an ideal case of 44.5 mA/cm^2 assuming a perfect antireflection surface, i.e. R=0% in the whole studied wavelength range.

2.3 Surface passivation

In order to determine the surface passivation quality of our samples we performed minority-carrier lifetime measurements as a function of the excess carrier density Δn through the quasi-steady-state photoconductance (QSS-PC) decay method using the WCT-120 apparatus (Sinton Instruments). Effective surface recombination velocity S_{eff} is a good indicator of surface passivation. This parameter can be calculated easily from lifetime measurements in symmetrical samples using

$$\frac{1}{\tau_{eff}} - \frac{1}{\tau_{in}} \cong \frac{2S_{eff}}{w} \quad (2)$$

where τ_{eff} is the measured effective lifetime, w the current wafer thickness, and τ_{in} is the intrinsic bulk lifetime (due to Auger and radiative recombination mechanisms) according to the parameterization by Richter et al. [20]. Trap assisted Shockley-Read-Hall SRH bulk recombination mechanism can be neglected in the study due to the high quality of the wafers.

As it can be seen in fig. 3a, reference samples achieve lifetimes over 3 ms at low injection levels independently of the doping polarity indicating a very efficient surface passivation with S_{eff} values below 5 cm/s at $\Delta n=10^{15}$ cm^{-3} (see Fig. 3b). Surprisingly b-Si samples achieve also very low S_{eff} values, well below 20 cm/s (<5 cm/ s for n-type substrate), despite the very unfavorable aspect ratio of the nanostructures compared with random pyramids resulting in a greatly increased total surface value.

<Fig.3>

Table I summarizes S_{eff} results in all analyzed samples. Especially remarkable surface passivation is obtained in the b-Si n-type sample yielding a S_{eff} of 4.8 cm/s, practically the same as the reference.

<Table I>

Reflectance and surface passivation results achieved in our precursors demonstrate the high potential of b-Si nanostructures, especially in n-type substrates, to be used for high efficiency solar cell fabrication. Regarding IBC solar cells, front surface S_{eff} values as those shown in table I would allow to obtain photovoltaic efficiencies up to 24.0% using a conventional fabrication baseline process as it will be discussed in section 4.

3. IBC solar cell fabrication details

Black silicon and reference random pyramids textured IBC solar cells, were fabricated using p- and n-type <100> FZ c-Si 275±10 μm thick 4 inches wafers with 2±0.5 Ωcm resistivity. Cross sections of p- and n-type b-Si IBC cells are shown in Fig. 4a and 4b respectively.

<Fig.4>

Fabrication of IBC devices consist of high-temperature steps (dopant diffusions and thermal oxidations), photolithography and front surface passivation with ALD Al_2O_3 on b-Si or textured surfaces. Phosphorus and boron diffusions are the same independently of the substrate polarity, consequently base and emitter areas are defined by interchanging lithography masks.

The fabrication process flow for b-Si IBC cells is pointed out in fig. 5a, following the next main stages, namely: i) Boron diffusion at 1000ºC soak temperature (both sides) resulting in a sheet resistance R_{sh} of ~25 Ω/sq. ii) Isotropic etching (~2 μm etching depth) to define p+ base or emitter regions on p- or n-type substrates respectively. iii) Dry oxidation to grow a thermal SiO_2 to mask subsequent phosphorus diffusions. iv) n++ phosphorus diffusion at 900ºC (R_{sh} ~25 Ω/sq) to define a selective emitter in p-type substrates or a high doped base contact in n-type wafers. v) Light n+ phosphorus diffusion at 830ºC (R_{sh} ~100 Ω/sq). vi) Dry thermal oxidation at 1080ºC to grow 110 nm thick SiO_2 to be used as a back reflector layer. Additionally, this film serves to mask anisotropic etching of reference textured IBC cells. Sheet resistances at the end of the drive-in stage were about 10, 70 and 100 Ω/sq in n++, n+ and p+ doped regions respectively. vii) and viii) b-Si etching and ALD Al_2O_3 (20 nm thick) as explained in section 2.1. Reference IBC cells were textured with random pyramids using anisotropic etching. ix) After opening contact windows (250 μm contact pitch) at the middle of each base and emitter finger, Aluminum was evaporated by e-beam both at the rear (~2 μm) and front sides (~0.5 μm). This last metal layer clearly defines the active area (see Fig. 5c). Metal is patterned using standard photolithography to define both interdigitated electrodes at the backside (see Fig. 3b) and light windows at the front surface. x) Finally a forming gas annealing at T=400ºC during 10 min is performed to recover e-beam damage [21] and activate Al_2O_3 surface passivation [22].

<Fig.5>

4. Results and discussion

Four wafers were processed, two p-type and two n-type, two using b-Si and two randomly textured reference IBC cells. In each wafer four 3 cm × 3 cm topologies were designed with different emitter coverage f_e, (i.e. emitter to total active area ratio), covering a f_e range from 67% to 86%. Base and emitter busbars were placed outside active area in all devices.

Solar cells were measured using a solar simulator (ORIEL 94021A) and a 4142B (Agilent HP) I-V characteristics tracer under standard test conditions STC (AM1.5G 1 kW/m^2 solar spectrum T=25ºC). External quantum efficiencies curves were obtained with QX10 instrument using a 2 cm × 2 cm light beam and 0.1 suns bias light. The best b-Si cell and its reference counterpart were also measured (*I-V* and *EQE* curves) in an independent laboratory (Fraunhofer CalLab).

Measured photovoltaic parameters as a function of f_e for the b-Si and reference IBC solar cells are shown in Fig. 6. 3D simulation results using Sentaurus Device software (Synopsys® TCAD tool) of b-Si structures are also included in the study (see Appendix section to simulation details) considering both an aluminum thickness of d_{Al}=2 μm in the backside metallization grid and the ideal case neglecting ohmic losses in fingers and busbars, i.e $d_{Al}\rightarrow\infty$.

<Fig.6>

As can be seen in Fig 6a and Fig. 6b, if f_e is tuned adequately, we reach efficiencies up to 22.1% (f_e=80%) and 22.0% (f_e=75%) in p- and n-type fabricated b-Si cells respectively. Table II summarizes photovoltaic parameters of the best b-Si cells, and its reference counterparts.

<Table II>

Excellent experimental short current density J_{sc} values about 41 mA/cm^2, in both substrate polarities, indicate that a good front surface passivation is achieved in our nanostructures in agreement with high lifetime results of our test samples (see section 2). 3D simulations -see Fig. 6 and results enclosed in parenthesis in table II- envisage efficiencies up to 24.0%, with J_{sc}, open circuit voltages, V_{oc}'s, and fill factors, *FF*'s, of 42.0±0.5 mA/cm^2, 675±15 mV and 83.0±1% ($d_{Al}\rightarrow\infty$) respectively, independent of base doping. Experimental results are very close to the simulated values. However, *FF* is the parameter we might improve in future runs by increasing aluminum thickness d_{Al} or using a two level metallization scheme, i.e. $d_{Al}\rightarrow\infty$. Specific series resistance due to fingers and busbars is estimated to be about 0.6-0.8 Ωcm^2 in our current devices. By doubling Al thickness we can achieve specific resistances well below 0.4 Ωcm^2 increasing *FF* beyond 82%. Additionally, V_{oc}'s values in n-type IBC cells are clearly lower than in p-type cells possibly due to technological issues leading to poorly passivated surface at p+ boron regions (emitter or back surface field regions on n- and p-type devices respectively). This fact might explain the general trend observed in the V_{oc} curves in Fig 6c,d (experimental and simulated results), i.e. the larger relative size of the p+ region the lower V_{oc} value. Hence, best fitting between simulations and experimental results in the f_e 50-90% range requires higher surface recombination at p+ than at n+ surfaces ($S_{pas,p+}$ = 5×10^4 cm/s compared with $S_{pas,n+}$ 1×10^3 cm/s). As a consequence optimum emitter coverage f_e has to be lower in n-type devices than in p-type ones. In fact, simulations foresee f_e < 60% as the best choice when n-type substrates are used.

Measured external quantum efficiency *EQE* curves for the best b-Si cells on n- and p-type IBC devices with the corresponding reference counterparts are shown in Fig. 7. Simulated *EQE* results for b-Si cells using the front surface recombination velocity values measured on our test samples (see table I) are also included (solid lines) in the study.

<Fig.7>

Agreement between simulated and measured *EQE* values indicates that the excellent front surface passivation is preserved in our finished devices, leading to an *EQE* over 95% in the 400-1000 nm λ range in all cases in agreement with J_{sc} electrical results. Experimental *EQE* curves in b-Si and reference n-type devices are quite similar at λ ~600 nm (see Fig. 7b), confirming that the b-Si surface reaches the same low level of surface recombination as textured one.

Experimental J_{sc} values differ from the theoretical $J_{sc,max}$ ~43.5 mA/cm^2 (see section 2.2) by the slight drop about 5% in *EQE* in the 300-1000 nm wavelength range compared with an ideal *EQE*=100%. Notice that every 1% drop in *EQE* of our b-Si IBC cells decreases J_{sc} about 0.4 mA/cm^2. The drop in photocurrent is partly related to internal quantum efficiency, *IQE*, losses by recombination either at the front surface or at non-doped and doped base (back surface field BSF) regions at the backside. However an unexpected high drop of J_{sc} occurs for f_e>75% in our n-type devices, as compared to the general trend of simulated J_{sc} values with f_e (see inset of Fig 6d). In order to clarify the origin of these J_{sc} losses, we have studied the effect of emitter coverage on *EQE* curves (see inset in Fig. 7b). Surprisingly in n-type cells *EQE* decreases with increasing f_e while the contrary occurs with much less overall variation in p-type devices. This anomalous behavior of our n-type devices might be related to lattice damage during boron diffusion [23, 24] resulting in a lower lifetime zone surrounding p+ regions.

5. Conclusions

This work demonstrates the viability of applying black silicon etching together with ALD Al_2O_3 surface passivation in both n- and p-type IBC solar cells. Very low reflectance values below 0.7% in the 300-1000 nm wavelength range with striking surface recombination velocities about 17 and 5 cm/s on p- and n-type substrates, respectively, are achieved. The last result, very similar value to the one reached on a conventional surface with random pyramids passivated with 90 nm of ALD Al_2O_3, confirms the high potential of b-Si on high efficiency n-type IBC solar cells. Outstanding photovoltaic efficiencies around 22% are achieved in the fabricated b-Si IBC cells independently of the substrate polarity. Even higher efficiencies up to 24.0% are expected in following runs by reducing series resistance of the rear metallization

grid and improving both surface passivation and bulk quality of our diffused boron p+ regions.

Acknowledgements

This work was partially supported by the Spanish MINECO (PCIN-2014-055) and Finnish TEKES (40329/14) agencies under Solar-Era.Net FP7 European Network. Dr. Trifon Trifonov is acknowledged for his help and comments to perform reflectance measurements and SEM/FIB images. Part of the research was performed at the Micronova Nanofabrication Centre, supported by Aalto University. G.G. acknowledges the research foundation of Helsinki University of Technology for funding the researcher exchange to UPC and Effinano project funded by School of Electrical Engineering at Aalto University.

Appendix. b-Si IBC solar cell 3D simulation details

Black silicon b-Si IBC solar cells have been simulated as a repetition of a simple domain, so-called unit cell, reducing simulation time and hardware computational requirements. In fig. 8 the simulated unit cell is shown. Notice that edge effects are neglected in the simulations.

<Fig.8>

The simulated unit cell is simplified as follows: i) all contacts are square shaped with a width $2\times r_c$ =60 μm and placed at the middle of base and emitter fingers with a pitch, p, of 250 μm- resulting in a locally contacted structure. ii) The wafer thickness w was set to w=275 μm. iii) S_F and S_R are the effective surface recombination velocities at the front and rear non-doped surfaces respectively. S_F value was adjusted accordingly to the values of table I, whereas S_R was always set to 10 cm/s. iv) p+ boron and n+ phosphorus diffusions are defined in a strip-like fashion with widths L_{p+} and L_{n+} respectively with a gap between regions of gap=40 μm. Additionally, we include a square n++ phosphorus doped region surrounding the corresponding contact width $2\times L_{n++}$=120 μm. By varying

L_{p+} or L_{n+} from a minimum value of 105 μm, we can adjust emitter coverage f_e on n-type or p-type substrates respectively. Gaussian doping profiles are considered for the n+, n++ and p+ doped regions with junction depths of 1.4, 2.5 and 5 μm respectively. Additionally, the peak doping N_s for n+ and p+ diffusions was set 1×10^{19} cm^{-3} in both cases, and 7×10^{19} cm^{-3} for the n++ region. Doping profile parameters are consistent with simulations of our baseline fabrication process using SUPREM (Stanford University Process Engineering Modeling) software. v) Surface recombination velocity of n+, n++ at non-contacted regions $S_{pas,n+}$ and $S_{pas,n++}$ were adjusted to 1×10^3 and 7×10^3 cm/s respectively accordingly Cuevas et al. parameterization [25]. $S_{pas,p+}$ was set to 5×10^4 cm/s. This last value is representative of a boron p+ surface with a peak doping of ~10^{19} cm^{-3} and passivated with an annealed thermal SiO_2 grown in chloride atmosphere once surface passivation is stabilized in time [26]. vi) Surface recombination velocity at the contacts was set to the thermal velocity limit ($S_{c,p+}$=$S_{c,n++}$=5×10^6 cm/s) as boundary condition. vii) Bulk recombination is limited by intrinsic mechanisms (Auger and radiative recombination), which is modelled using the parameterization given in [19]. Additionally trap-assisted Shockley-Read-Hall SRH recombination is neglected in the study (the related lifetime is set to 1 s). viii) The nanostructured front surface is replaced by a flat polished surface with total optical transmission (T=100%) and considering simultaneously a modified AM1.5G spectral irradiance S_{mod} =$S(\lambda)\times(1-R(\lambda))$ as incident light. Here, $S(\lambda)$ is the spectral irradiance of the standard AM1.5G solar spectrum and $R(\lambda)$ is the measured reflectance of the b-Si IBC precursor shown in Fig. 2. Additionally, an internal front and rear reflectance of R_{int_front}=100% and $<R_{int\_rear}>$ respectively are introduced in the simulations. The last parameter is adjusted for each emitter coverage taking into account the metallization gap between base and emitter electrodes gap_{met}=80 μm, an internal reflection of 96% for metallized non-contacted areas, and 85% for contacted and non-metallized areas. The former value corresponds to an ideal back reflector using an optimized Al/SiO_2 stack. The last value arises from the best fitting between simulated and measured *EQE* curves in the 1050-1150 nm wavelength range for all emitter coverage f_e range (60-86%). ix) Flat bands have been considered at the passivated non-doped semiconductor surfaces, i.e. neither dielectric charge nor metal-insulator-semiconductor interface are considered in the simulations. Therefore, there are no inversion or accumulation layers below passivated surfaces. x) Physical models - e.g. carrier statistics, band gap narrowing, and carrier mobilities - are

the same as considered in [27]. xi) Ohmic losses related to the backside metallization grid (fingers and busbars) are modelled by a lumped series resistance R_s in Ω units whose value is:

$$R_S \cong \frac{R_{sh,Al}}{3} \cdot \left(\frac{1}{f_{m,b}} + \frac{1}{f_{m,e}} + \frac{1}{f_{m,bus}} \right) \cdot \frac{A}{A_i} \tag{3}$$

where A and A_i is the total cell and simulated unit cell area respectively, $f_{m,b}$, $f_{m,e}$, $f_{m,,bus}$ are the metallization factors due to base and emitter fingers and busbars respectively. $R_{sh,Al}$ is the metal sheet resistance which is evaluated taking into account the aluminum resistivity ρ_{Al} 2.8×10^{-6} Ωcm and the metal layer thickness d_{Al} as $R_{sh,Al}=\rho_{Al}/d_{Al}$. Notice that $f_{m,b}$ and $f_{m,e}$ changes accordingly with emitter coverage considering current L_{p+}, L_{n+} values and the gap between electrodes gap_{met} as follows:

$$f_{m,b} = \frac{L_{p+} - E_{gap,met}/2}{L_{p+} + L_{n+} + E_{gap,met}} \tag{4}$$

$$f_{m,e} = \frac{L_{n+} - E_{gap,met}/2}{L_{p+} + L_{n+} + E_{gap,met}} \tag{5}$$

$f_{m,bus}$ was always set to 0.133 independent of f_e. Additionally, the contact resistance between metal and high doped contacted regions is neglected in the simulations.

References

[1] Sinton RA, Swanson RM. Simplified backside-contact solar cells. *IEEE Trans. Electron Devices* 1990; **37**(2): 348-352.

[2] Franklin E, Fong K, McIntosh K, Fell A, Blakers A, Kho T, Walter D, Wang D, Zin N, Stocks M, Wang E, Grant N, Wan Y, Yang Y, Zhang X, Feng Z, Verlinden P.J. Design, fabrication and characterisation of a 24.4% efficient interdigitated back contact solar cell. *Progress in Photovoltaics: Research and Applications* 2014; DOI:10.1002/pip.2556.

[3] Glunz S.W. High efficiency crystalline silicon solar cells. *Advances in OptoElectronics* 2007; **2007**; 1-15.

[4] Masuko K, Shigematsu M, Hashiguchi T, Fujishima D, Kai M, Yoshimura N, Yamaguchi T, Ichihashi Y, Mishima T, Matsubara N, Yamanishi T, Takahama T, Taguchi M, Maruyama E, Okamoto S. Achievement of more than 25% conversion efficiency with crystalline silicon heterojunction solar cell. *IEEE Journal of Photovoltaics* 2014; **4**(6); 1433-1435.

[5] Reichel C, Graneck F, Hermle M, Glunz S.W. Back-contacted back-junction n-type silicon solar cells featuring an insulating thin film for decoupling charge carrier collection and metallization geometry. *Progress in Photovoltaics: Research and Applications* 2013; **21**;1063-1076.

[6] Carrió D, Ortega P, Martín I, López G, López-González J.M, Orpella A, Voz C, Alcubilla R. Rear contact pattern optimization based on 3D simulations for IBC solar cells with point-like doped contacts. *Energy procedia* 2014; **55**; 47-52.

[7] Yuan H.C, Yost E, Page M.R, Stradins P, Meier D.L, Branz H.M. Efficient black silicon solar cell with a density-graded nanoporous surface: optical properties, performance limitations, and design rules. *Applied Physics Letters* 2009; **95**; 123501.

[8] Savin H, Repo P, Von Gastrow G, Ortega P, Calle E, Garín M, Alcubilla R. Black silicon solar cells with interdigitated back-contacts achieve 22.1% efficiency. *Nature nanotechnology* 2015; Published online. DOI: 10.1038/NNANO.2015.89.

[9] Hoex B, Schmidt J, Pohl P, Van de Sanden M.C.M, Kessels W.M.M. Silicon Surface passivation by atomic layer deposition Al_2O_3. *Journal of Applied Pysics* 2008; 104; 044903.

[10] Dingemans G, Kessels W.M.M. Status and prospects of Al2O3-based surface passivation schemes for silicon solar cells. *Journal of Vacuum Science and Technology A* 2012; **30**(4); 040802-1.

[11] Repo P, Haarahiltunen A, Sainiemi L, Yli-Koski M, Talvitie H, Shubert M. C, Savin H, "Effective passivation of black silicon surfaces by atomic layer deposition", *IEEE Journal of Photovoltaics* 2013; **3**(1), 90-94.

[12] Allen T, Bullock J, Cuevas A, Baker-Finch S, Karouta F. Reactive ion etched black silicon texturing: a comparative study. *Proc. of 40th IEEE Photovoltaic Specialist Conference*, Denver (USA), 2014; 562-566.

[13] Von Gastrow G, Alcubilla R, Ortega P, Yli-koski M, Conesa-Boj S, Fontcuberta i Morral A, Savin H. Analysis of the atomic layer deposited Al_2O_3 field-effect passivation in black silicon. *Solar Energy Materials & Solar cells* 2015; Published online. DOI: 10.1016/j.solmat.2015.05.027.

[14] López G, Ortega P, Voz C, Martín I, Colina M, Morales-Vilches A, Orpella A, Alcubilla R. Surface passivation and optical characterization of Al_2O_3/a-SiC_x stacks on c-Si substrates. *Beilstein Journal of Nanotechnoly* 2013; **4**:726-731.

[15] Otto M, Algasinger M, Branz H, Gesermann B, Gimpel T, Füchsel K, Käsebier T, Kontermann S, Koynov S, Li X, Naumann V, Oh J, Sprafke A. N, Ziegler J, Zilk M, Wehrspohn. Black silicon photovoltaics. *Advanced optical materials* 2014. Published online. DOI: 10.1002/adom.201400395.

[16] Mews M, Leendertz C, Algasinger M, Koynov S, Korte L. Amorphous/crystalline silicon heterojunction solar cells with black silicon texture. *Physics Status Solidi RRL* 2014; **8**(10): 831-835.

[17] Jeong S, McGehee M.D, Cui Y. All-back-contact ultra-thin silicon nanocone solar cells with 13.7% power conversion efficiency. *Nature communications* 2013; **4**; 2950.

[18] Glunz, S.W, Rein S, Warta W, Knobloch J, Wettling W. On the degradation of Cz-silicon solar cells. *Proc. of 2nd World Conference and Exhibition on Photovoltaic Solar Energy Conversion*, Vienna (Austria), 1998; 1343-1346.

[19] Ingenito A, Isabella O, Zeman M. Experimental demonstration of $4n^2$ classical absorption limit in nanotextured ultrathin solar cells with dielectric omnidirectional back reflector. *ACS photonics* 2014; **1**: 270-278.

[20] Richter A, Glunz S.W, Werner F, Schmidt J, Cuevas A. Improved quantitative description of Auger recombination in crystalline silicon. *Physical Review B* 2012; 86; 165202.

[21] Coll A, Martín I, Ortega P, Bermejo S, López G, Alcubilla R. Impact of metallization techniques on Surface passivation of high efficiency crystalline silicon solar cells. *Proc. of 28th European Photovolatic Solar Energy Conference*, Paris (France), 2013; 1213-1216.

[22] López G, Ortega P, Voz C, Martín I, Colina M, Orpella A, Alcubilla R. Optimization of Al_2O_3 films obtained by ALD to passivate p-type c-silicon wafers. *Proc. of 27th European Photovolatic Solar Energy Conference*, Frankfurt (Germany), 2012; 1692-1695.

[23] Cousins P. J, Cotter J. E. The influence of diffusion-induced dislocations on high efficiency silicon solar cells. *IEEE Transaction on Electron Devices* 2006; 53(3); 457-464.

[24] Kessler M.A, Ohrdes T, Wolpensinger B. Charge carrier lifetime degradation in Cz silicon through the formation of a boron rich layer during BBr_3 diffusion processes. *Semiconductor Science and Technology* 2010; **25**; 055001.

[25] Cuevas A, Basore P.A, Giroult-Matlakowski G, Dubois C. Surface recombination velocity of highly doped n-type silicon. *Journal of Applied Pysics* 1996; 80; 3370.

[26] Altermatt P.P, Plagwitz H, Bock R, Schmidt J, Brendel R, Kerr M.J, Cuevas A. The surface recombination velocity at boron-doped emitters: comparison between various passivation techniques. *Proc. of 21st European Photovolatic Solar Energy Conference*, Dresden (Germany), 2006; 647-650.

[27] López-González J.M, Martín I, Ortega P, Orpella A, Alcubilla R. Numerical simulations of rear point-contacted solar cells on 2.2 Ωcm p-type c-Si substrates. *Progress in Photovoltaics: Research and Applications* 2015; **23**;69-77.

Table I. S_{eff} values evaluated at $\Delta n=10^{15}$ cm^{-3} for both p- and n-type substrates considering random pyramids textured or black silicon morphologies.

	p-type b-Si	*p-type* random	*n-type* b-Si	*n-type* random
S_{eff} (cm/s)	16.7	3.2	4.8	4.8

Table II. Best results under STC conditions (AM1.5G 1 kW/m^2 solar spectrum T=25°C) for b-Si and their reference cells on n-type and p-type substrates (9 cm^2 cell area). Values enclosed in parenthesis correspond to simulated results with $d_{Al} \rightarrow \infty$.

Cell	f_e (%)	J_{sc} (mA/cm^2)	V_{oc} (mV)	FF (%)	η (%)
b-Si (p-type) (*)	**80**	**41.0 (41.4)**	**678 (684)**	**79.5 (83.0)**	**22.1 (23.5)**
Ref. (p-type) (*)	80	41.4	679	78.9	22.2
b-Si (n-type)	**75**	**40.9 (41.5)**	**662 (661)**	**81.3 (83.9)**	**22.0 (23.0)**
Ref. (n-type)	75	40.3	645	80.7	21.0

(*) These cells were measured in an independent laboratory (Fraunhofer ISE CalLab).

Figure Captions

Figure 1. a), c) FIB/SEM images of silicon surface after b-Si and random pyramids etching respectively. b), d) A close view showing b-Si and random pyramid surface morphologies respectively. Notice that fig a) and d) have the same scale.

Figure 2. Front reflectance measured in two p-type precursors with b-Si and random textured surfaces passivated with ALD Al_2O_3. Samples include a back reflector scheme of SiO_2 (110 nm)/Al (2 μm). Spectral photon flux density considering AM1.5G solar spectrum $\phi_{AM1.5}$ is also depicted in the graph.

Figure 3. a) Effective lifetime and b) effective surface recombination velocity measurements vs. excess carrier density Δn on b-Si (open symbols) and random (filled symbols) p-type and n-type substrates. p-type data are the same as reported in [8].

Figure 4. Cross section sketches of a) p- and b) n-type b-Si IBC solar cells.

Figure 5. a) Fabrication process flow for n- and p-type b-Si IBC cells. Images of a manufactured 4 inches wafer at the end of the fabrication process showing b) rear and c) front surfaces. Each wafer contains four 9 cm^2 devices with different emitter coverage 67%, 75%, 80% and 86%.

Figure 6. a), b) Measured values of efficiency η, c), d) V_{oc} and e), f) *FF* vs. emitter coverage f_e of b-Si (open symbols) and reference (filled symbols) IBC solar cells on p- (left) and n-type substrates (right). Dashed lines correspond to simulated efficiencies taking into account aluminum thickness of the backside metallization grid, d_{Al}. Short-circuit current density J_{sc} is also shown in the insets of e) and f). Note, that the b-Si p-type cell with f_e=75% failed, therefore the corresponding values are missing in the graphs.

Figure 7. a) External quantum efficiencies *EQE*'s of best p-type b-Si IBC solar cell (f_e=80%) and its reference counterpart. *EQE* data of both curves were measured in an independent laboratory (Fraunhofer ISE CalLab). b) *EQE*'s of best n-type b-Si cell (f_e=75%) and its reference counterpart. Experimental *EQE* curves for several f_e's are also shown in the insets. Solid lines in a) and b) correspond to 3D simulations of b-Si cells considering the front surface recombination velocities of our precursors of Table I.

Figure 8. Sketch of the simulated structure: a) 2D cross section and b) bottom view.

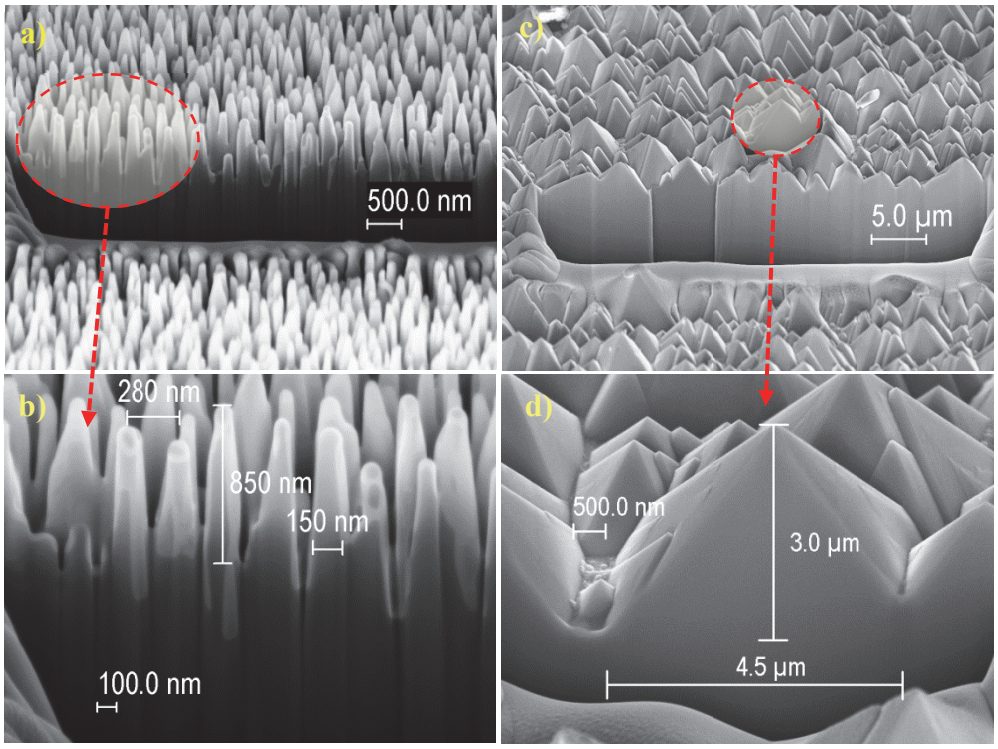
a)
500.0 nm
c)
5.0 μm
b)
280 nm
850 nm
150 nm
100.0 nm
d)
500.0 nm
3.0 μm
4.5 μm

<Fig. 1>

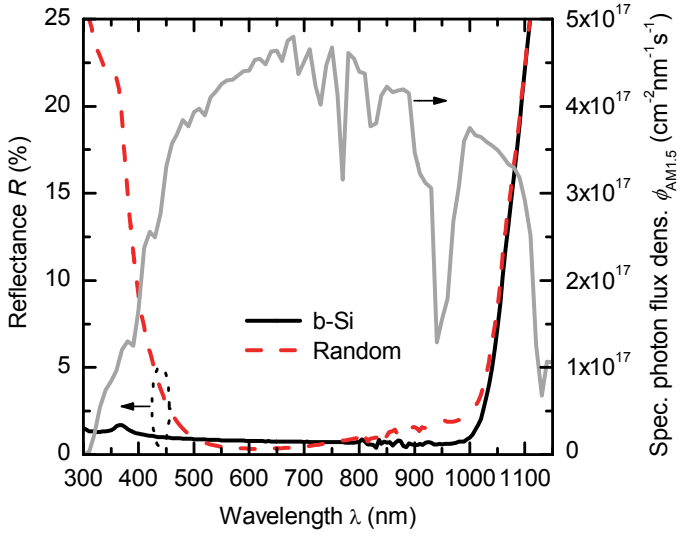
Reflectance R (%)
Spec. photon flux dens. $\phi_{AM1.5}$ ($cm^{-2}nm^{-1}s^{-1}$)
Wavelength λ (nm)
b-Si
Random
0
5
10
15
20
25
300
400
500
600
700
800
900
1000
1100
0
1x10^17
2x10^17
3x10^17
4x10^17
5x10^17

<Fig. 2>

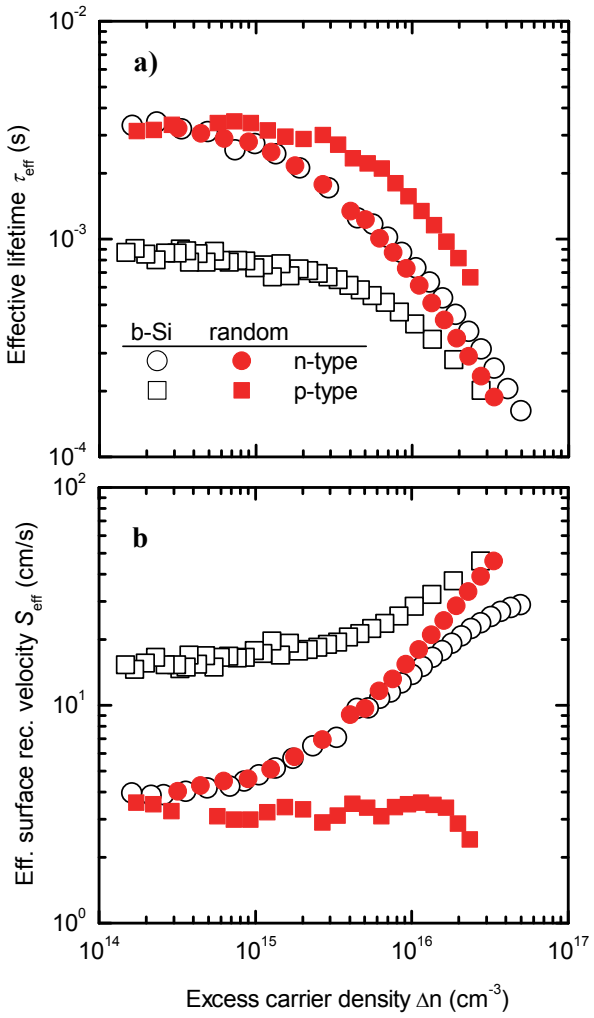
a)
b
b-Si
random
n-type
p-type
Effective lifetime τ_{eff} (s)
Eff. surface rec. velocity S_{eff} (cm/s)
Excess carrier density Δn (cm^{-3})
10^{-2}
10^{-3}
10^{-4}
10^{2}
10^{1}
10^{0}
10^{14}
10^{15}
10^{16}
10^{17}

<Fig.3>

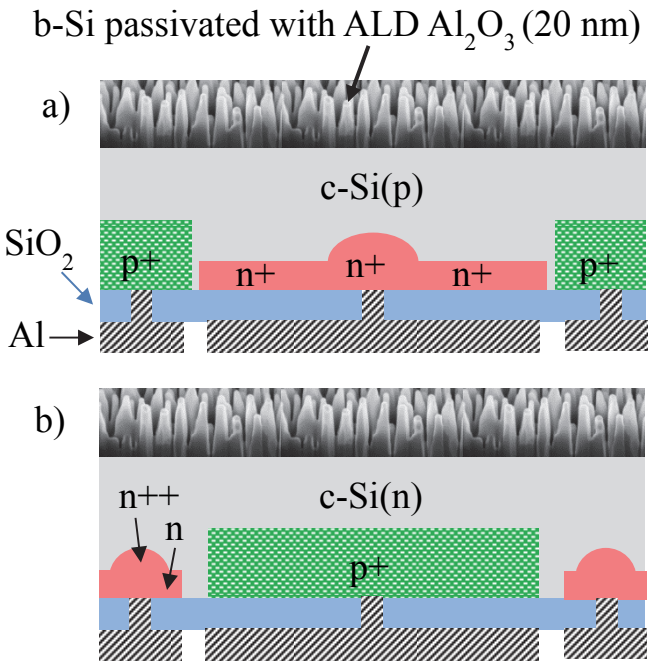
b-Si passivated with ALD Al_2O_3 (20 nm)
a)
c-Si(p)
SiO_2
p+
n+
n+
n+
p+
Al
b)
n++
n
c-Si(n)
p+

<Fig. 4>

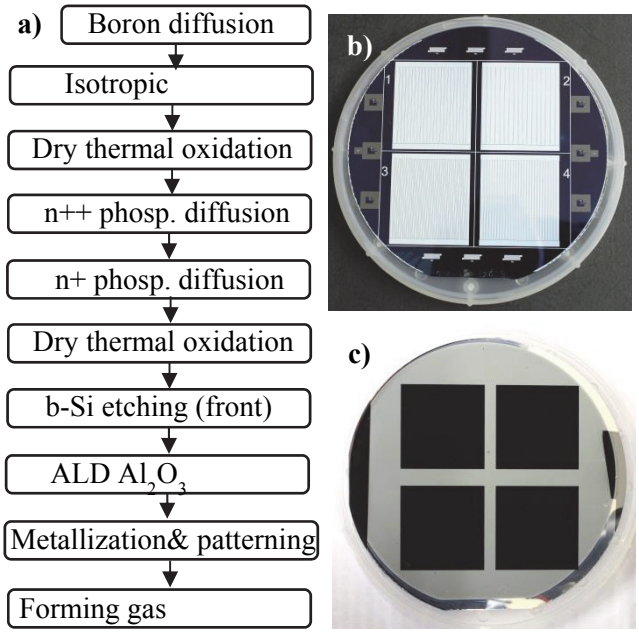
a)
Boron diffusion
Isotropic
Dry thermal oxidation
n++ phosp. diffusion
n+ phosp. diffusion
Dry thermal oxidation
b-Si etching (front)
ALD Al_2O_3
Metallization& patterning
Forming gas
b)
1
2
3
4
c)

<Fig. 5>

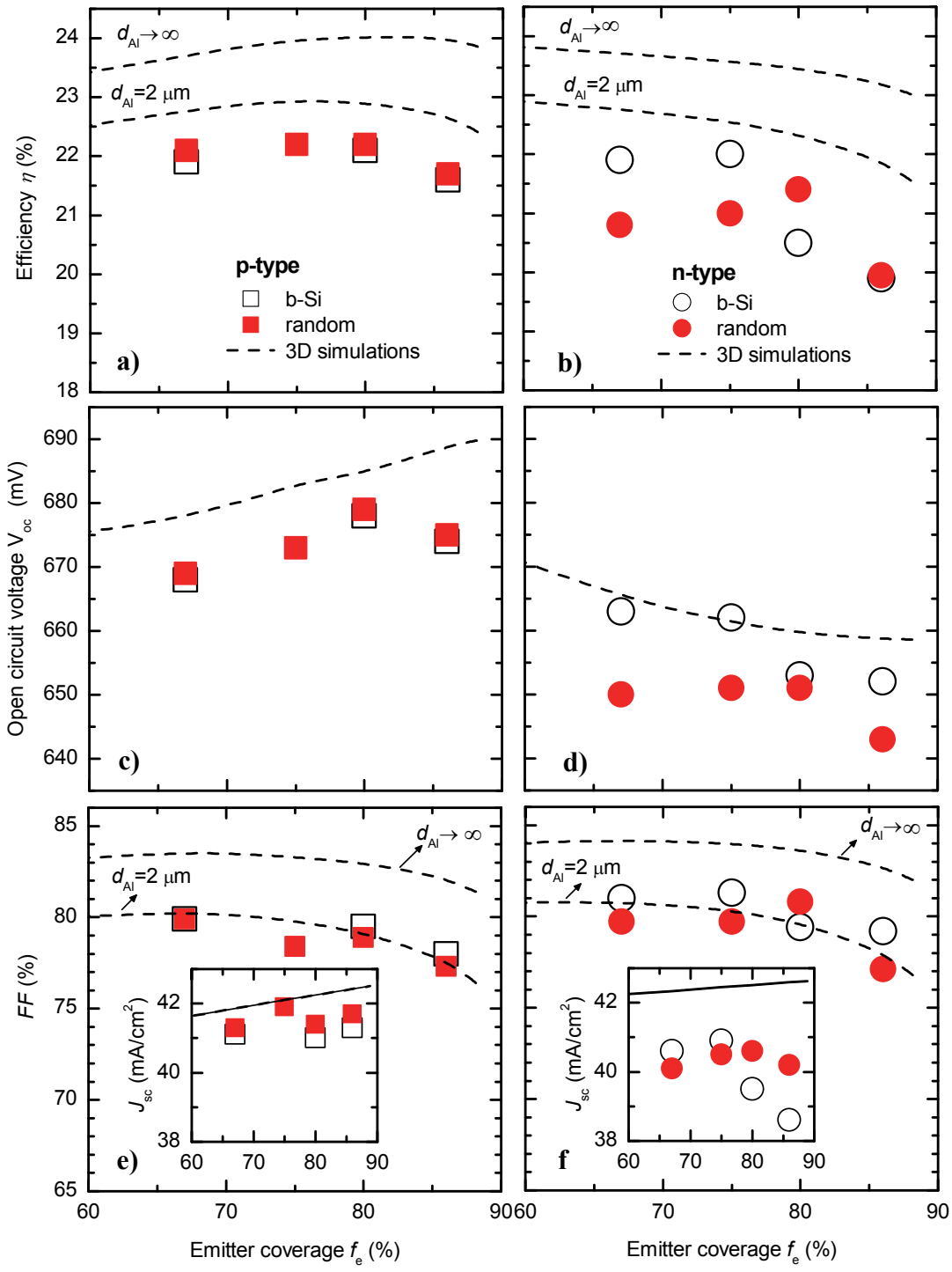
Efficiency η (%)
Open circuit voltage V_oc (mV)
FF (%)
J_sc (mA/cm²)
d_Al→∞
d_Al=2 μm
p-type
n-type
b-Si
random
3D simulations
a)
b)
c)
d)
e)
f
Emitter coverage f_e (%)
Emitter coverage f_e (%)

<Fig. 6>

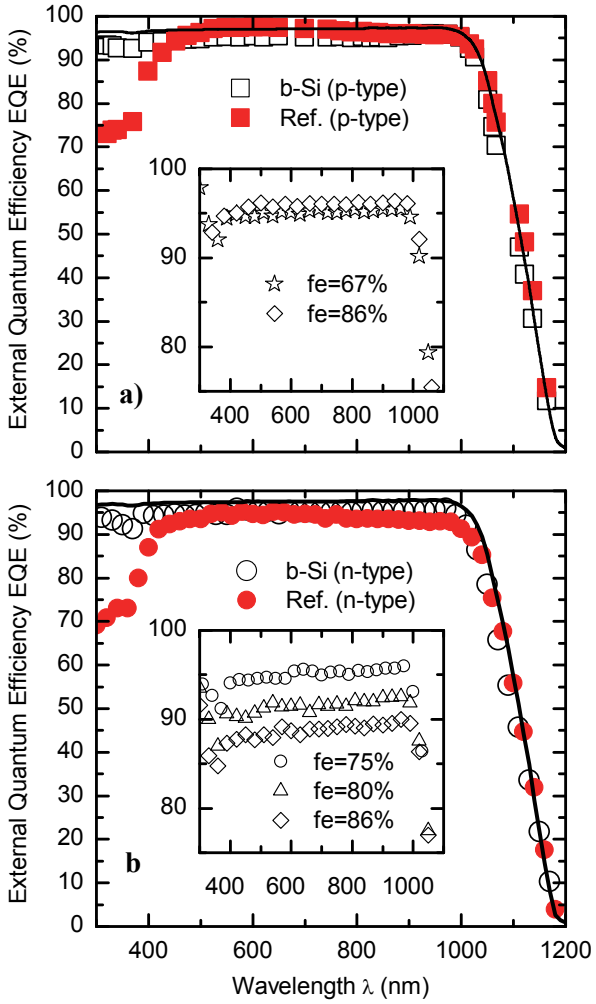
External Quantum Efficiency EQE (%)
b-Si (p-type)
Ref. (p-type)
fe=67%
fe=86%
a)
b-Si (n-type)
Ref. (n-type)
fe=75%
fe=80%
fe=86%
b
Wavelength λ (nm)

<Fig. 7>

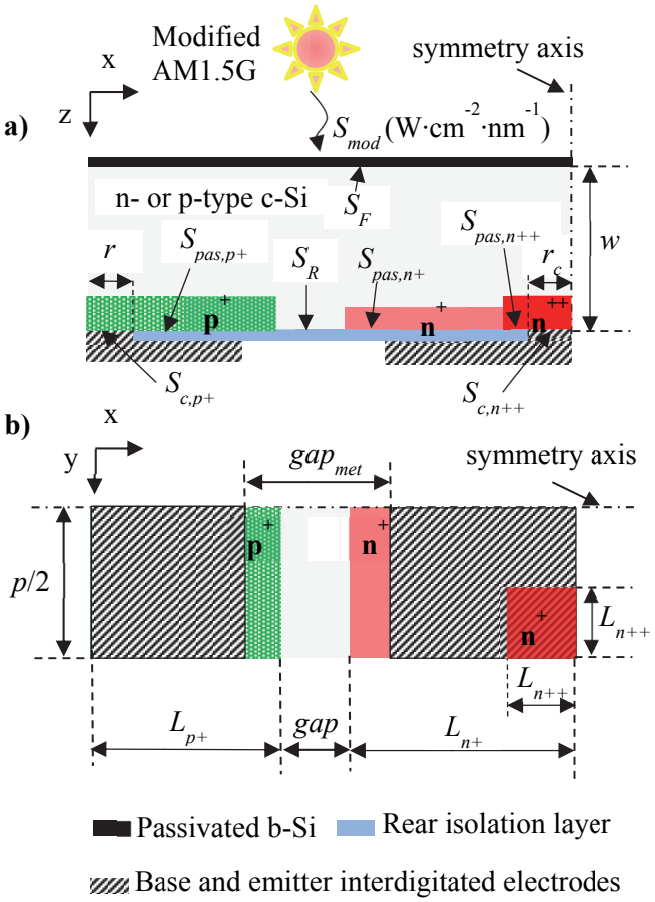
a)
Modified
AM1.5G
x
z
symmetry axis
S_{mod} (W·cm^{-2}·nm^{-1})
n- or p-type c-Si
S_F
$S_{pas,p+}$
S_R
$S_{pas,n+}$
$S_{pas,n++}$
r
r_c
w
p
n
n
$S_{c,p+}$
$S_{c,n++}$
b)
x
y
gap_{met}
symmetry axis
$p/2$
p
n
n
L_{n++}
L_{n++}
L_{p+}
gap
L_{n+}
Passivated b-Si
Rear isolation layer
Base and emitter interdigitated electrodes

<Fig. 8>